

# Understanding the invisible through numerical simulation of wave propagation

Hélène Barucq <sup>1</sup>.

SMAI 2023 – Le Gosier, Guadeloupe – May 2023

The Inria logo is written in a red, cursive script.The MAKUTU logo consists of the word "MAKUTU" in a bold, black, sans-serif font. Each letter is filled with a complex, white, fractal-like pattern.

---

<sup>1</sup>Project-Team Makutu, Inria–TotalEnergies–UPPA, LMAP, UMR CNRS 5142

# Table of Contents

- 1 Introduction
- 2 Energy Geophysics
- 3 Illustration: Elastic wave propagation with HDG
  - Mathematical formulation and HDG algorithm
  - Illustration of gains
- 4 Inverse problem
  - Iterative minimization algorithm
  - Numerical experiment
- 5 Helioseismology/asteroseismology
- 6 Illustration: Green's function computations for time-distance helioseismology
  - Modal Green's kernel
  - Numerical experiments
  - Power spectrum, comparison with measured data
  - The vector wave problem
- 7 Conclusion

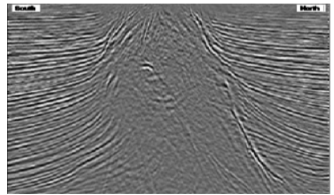
# Plan

## 1 Introduction

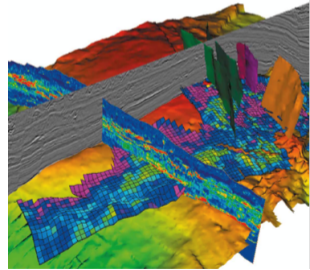
# Broad scientific context

Describe a place with exactness from more or less numerous and precise memories, or guessing the content and internal structures of an object after having observed it only partially, without ever touching it because it is inaccessible or very fragile?

- ① Wave propagation is helping
- ② Waves are very sensitive to any change in the propagation medium.



(a) Seismogram.



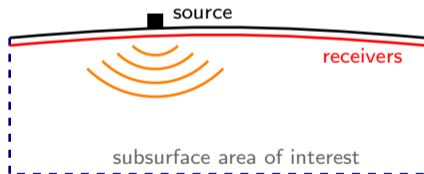
(b) Reservoir model.

# Inverse problems

Basically, inverse wave problems are composed of:

- 1 Emitting sources that will propagate through the medium and recording the reflected waves on a set of receivers; **acquisition/ forward problem**
- 2 From the acquisitions, find the propagation medium; **inverse problem/backward problem**

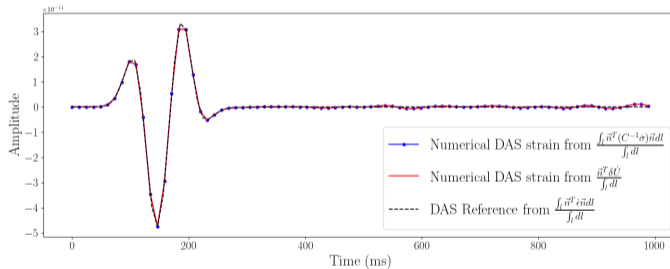
Example: Seismic imaging for the **Reconstruction/Monitoring** of subsurface Earth properties



- 1 **Accurate simulation of wave propagation in large-scale complex media,**
- 2 **Efficient procedure for nonlinear reconstruction of properties.**

# Numerical data match real data

Compare data with simulations: computationally and possibly timely expensive



Comparison of observation and numerical result

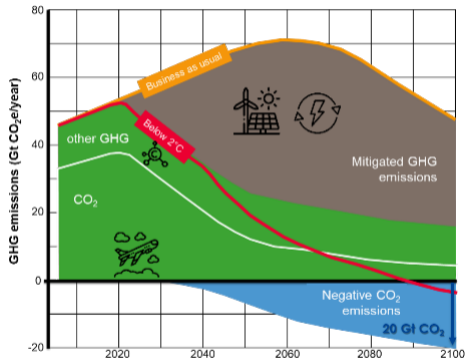
..

# Plan

## 2 Energy Geophysics

# Access to energy resources

- ▶ Hydrocarbons
- ▶ Geothermal
- ▶ Hydrogen



Source: The Emissions Gap Report 2017. United Nations Environment Programme (UNEP)

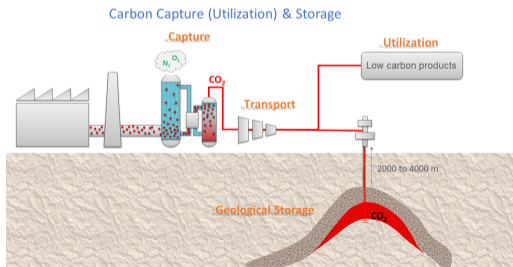


# Facilitate safe carbon capture, utilization and storage - CCUS

- ▶ CO<sub>2</sub> emissions: leading cause of climate change;
- ▶ Geological storage of CO<sub>2</sub>: important tool for the stabilization of atmospheric greenhouse gas concentrations;
- ▶ CO<sub>2</sub> is injected into underground geological formations; Safe, permanent, and effective.

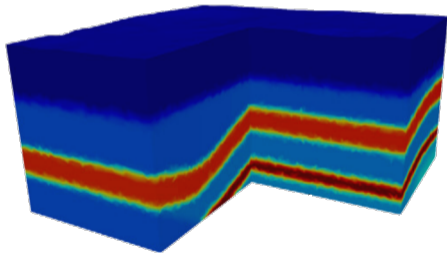
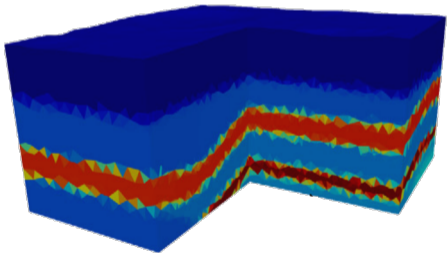
How do we ensure the safety and sustainability of storage?

That's where **seismic monitoring** comes into play.



# Research routine: propagation domains

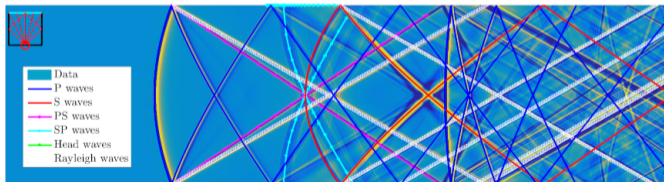
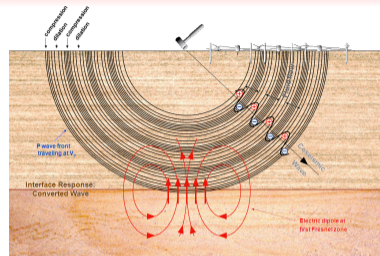
- ▶ 3D large domains
- ▶ topography, heterogeneity
- ▶ a network of sources whose number is of the order of several thousands



Parameterization matters

# Research routine: wave equations

- ▶ Acoustic wave equation,
- ▶ Elastic wave equation,
- ▶ Electromagnetic wave equation,
- ▶ Couplings



Waves in solid media

## Equations 2/2

Acoustic wave equation, time and frequency domains:

$$\left\{ \begin{array}{l} \rho \partial_t \mathbf{v}(\mathbf{x}, t) = -\nabla p(\mathbf{x}, t), \\ \frac{1}{c^2 \rho} \partial_t p(\mathbf{x}, t) + \nabla \cdot \mathbf{v}(\mathbf{x}, t) = 0. \end{array} \right. \quad \left\{ \begin{array}{l} -i\omega \rho \mathbf{v}(\mathbf{x}, \omega) = -\nabla p(\mathbf{x}, \omega), \\ -\frac{1}{c^2 \rho} i\omega p(\mathbf{x}, \omega) + \nabla \cdot \mathbf{v}(\mathbf{x}, \omega) = 0. \end{array} \right.$$

Elasto-dynamic equations, time and frequency domains:

$$\left\{ \begin{array}{l} \rho \partial_t \mathbf{v}(\mathbf{x}, t) = \nabla \cdot \underline{\underline{\sigma}}(\mathbf{x}, t), \\ \partial_t \underline{\underline{\sigma}}(\mathbf{x}, t) = \underline{\underline{C}}(\mathbf{x})(\underline{\underline{\epsilon}}(\mathbf{v})). \end{array} \right. \quad \left\{ \begin{array}{l} -i\omega \rho \mathbf{v}(\mathbf{x}, \omega) = \nabla \cdot \underline{\underline{\sigma}}(\mathbf{x}, \omega), \\ -i\omega \underline{\underline{\sigma}}(\mathbf{x}, \omega) = \underline{\underline{C}}(\mathbf{x})(\underline{\underline{\epsilon}}(\mathbf{v})). \end{array} \right.$$

## Equations 2/2

Each approach has pros and cons

### Time-domain formulation

- ▶ Using data is straightforward
- ▶ Matrix-free implementation relieves memory,
- ▶ frequency-dependent parameters,
- ▶ adjoint of the discrete problem can differ from discrete adjoint, additional developments are required,
- ▶ multi-sources

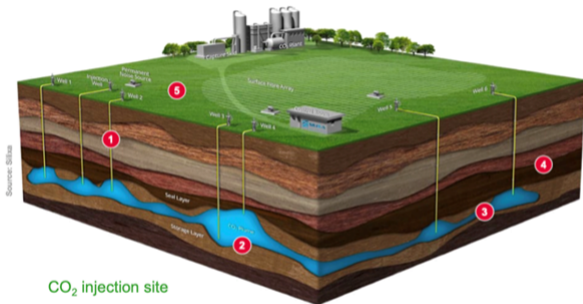
### Time-harmonic formulation

- ▶ Easily handle attenuation,
- ▶ multi-sources with direct solver,
- ▶ reuse matrix factorization for adjoint-problem in inversion,
- ▶ memory cost for matrix factorization with direct solver,

# Modelling and simulation challenges 1/2

## A multi-physics problem and...

- ✓ CO<sub>2</sub> sequestration and monitoring are more and more recognized as a key element in the path towards energy decarbonization
- ✓ CO<sub>2</sub> sequestration and monitoring is an excellent example gathering the leading-edge technology of many different domain to help in the prediction of the plume evolution:
  - ✓ Flow and geo-mechanical simulation,
  - ✓ Gravimetry,
  - ✓ Seismic modelling and inverse problem, monitoring acquisition technology,
  - ✓ In situ data visualization and analysis,
  - ✓ Machine learning
  - ✓ ...



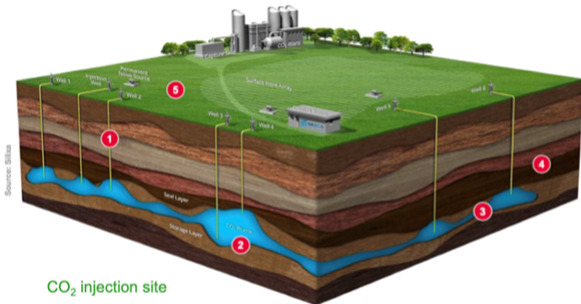
- 1 Well integrity/injectivity
- 2 Pressure/Stress change  
Fault Activation
- 3 CO<sub>2</sub> transport & trapping
- 4 Seal integrity
- 5 Surface deformation  
Seismicity

# Modelling and simulation challenges 2/2

## HPC Issue

- ✓ **Limitations:**
  - ✓ **Multiphysics: geomechanic+Flow+Seismic**
  - ✓ **Large Scale: 98% storage in Aquifer**
  - ✓ **Long Term Simulation: post injection matters**
- ✓ **Solutions:**
  - ✓ **Fast and scalable algorithms**
  - ✓ **Perennial solutions: portability**

**Target: Exascale Computers**

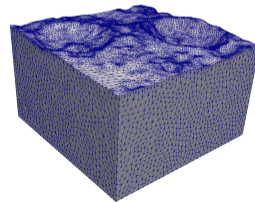
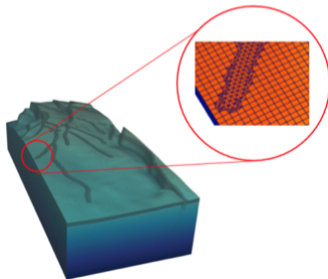
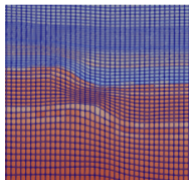


CO<sub>2</sub> injection site

- 1 Well integrity/injectivity
- 2 Pressure/Stress change  
Fault Activation
- 3 CO<sub>2</sub> transport & trapping
- 4 Seal integrity
- 5 Surface deformation  
Seismicity

# Numerical methods 1/2

- ▶ Finite Differences: implementation easy, low cost, inaccuracy for the topography
- ▶ Finite Elements: implementation possibly tricky, expensive, accurate for the topography
- ▶ Boundary integral equations: not efficient in highly heterogeneous media
- ▶ Semi-Analytical: lack of flexibility, geometrical effects, anisotropy neglected,



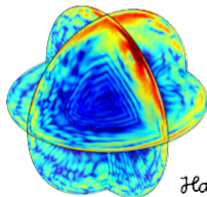


# In Makutu team 2/2

- ▶ Spectral element methods (SEM)
- ▶ Discontinuous Galerkin methods (DG)
- ▶ Non polynomial basis functions in Trefftz framework
  
- ▶ **Explicit** schemes in time
- ▶ High-order
- ▶ **hp-adaptivity** with DG



Multiphysics  
Simulator on HPC



*Hawen*

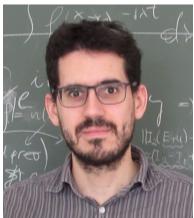
<https://ffaucher.gitlab.io/hawen-website/>

# Plan

- 3 Illustration: Elastic wave propagation with HDG
  - Mathematical formulation and HDG algorithm
  - Illustration of gains

# Elastic wave propagation with HDG

In collaboration with Florian Faucher and Ha Pham



# Plan

- 3 Illustration: Elastic wave propagation with HDG
  - Mathematical formulation and HDG algorithm
  - Illustration of gains

# Elastic wave problem

New sensing devices such as fiber optic measure strain ( $\epsilon$ ). Therefore, we want to solve for  $(\mathbf{u}, \boldsymbol{\sigma})$  to have maximum accuracy rather than replacing in terms of  $\mathbf{u}$  only.

$$\begin{cases} -\omega^2 \mathbf{u} - \nabla \cdot \boldsymbol{\sigma} = \mathbf{f}, \\ \boldsymbol{\sigma} = \frac{1}{2} \mathbf{C} : \boldsymbol{\epsilon}, \quad \boldsymbol{\epsilon} = (\nabla \mathbf{u} + \nabla^T \mathbf{u}), \end{cases} \quad (1)$$

The physical properties describing the medium are contained in the stiffness tensor  $\mathbf{C}$ .

Time-harmonic wave problems:

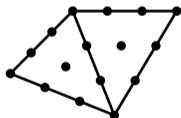
- + Easily encode the **attenuation** with complex-valued parameters,
- + Direct solvers allow for **multiple right-hand sides** once the factorization is obtained,
- **Memory cost** of the matrix factorization.

# HDG discretization

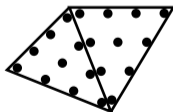
$$\begin{cases} -\omega^2 \mathbf{u} - \nabla \cdot \boldsymbol{\sigma} = \mathbf{f}, \\ \boldsymbol{\sigma} = \frac{1}{2} \mathbf{C} : (\nabla \mathbf{u} + \nabla^T \mathbf{u}), \end{cases}$$

## Hybridizable Discontinuous Galerkin method

- ▶ **Static condensation** on first-order DG Formulations **without** increasing the number of unknown: The unknown of the global matrix is **only** the numerical trace  $\hat{\mathbf{u}}$ .
- ▶ Handle **complex geometry** (topography) with *p*-adaptivity,
- ▶ Reduces the computational cost by removing inner dofs.



Finite Element



Discontinuous Galerkin



HDG



B. Cockburn J. Gopalakrishnan and R. Lazarov

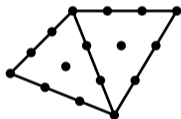
Unified hybridization of discontinuous Galerkin, mixed, and continuous Galerkin methods for second order elliptic problems

SIAM Journal on Numerical Analysis (47), 2009.

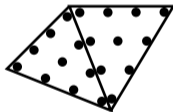
# HDG discretization

Hybridizable Discontinuous Galerkin method for the discretization

- ▶ Static condensation for first-order problems **without** increasing the number of unknowns: The unknown of the global matrix is **only** the numerical trace  $\hat{\mathbf{u}}$ .
- ▶ Handle **complex geometry** (topography) with *p*-adaptivity,
- ▶ Reduces the computational cost by removing inner dofs.



Finite Element



Discontinuous Galerkin



HDG

HDG is more efficient with high-order polynomial (order  $> 4$ ).  
High-order  $\Rightarrow$  Large cell  $\Rightarrow$  variable  $\mathbf{C}$  within cells for resolution.



## HDG Variational formulation (1/2): stiffness tensor version

The local problem is written on each cell  $K_e$  of the mesh, and the HDG problem is written in terms of  $(\mathbf{u}, \boldsymbol{\sigma}, \hat{u})$ . Using test-functions  $(\psi, \phi)$ ,

$$\left\{ \begin{array}{l} \int_{K_e} -\omega^2 \mathbf{u} \bar{\psi} - \int_{K_e} \nabla \cdot \boldsymbol{\sigma} \bar{\psi} = \int_{K_e} \mathbf{f} \bar{\psi}, \end{array} \right. \quad (2a)$$

$$\left\{ \begin{array}{l} \int_{K_e} \frac{1}{2} \mathbf{C} : \nabla \mathbf{u} \bar{\phi} + \int_{K_e} \frac{1}{2} \mathbf{C} : \nabla^T \mathbf{u} \bar{\phi} - \int_{K_e} \boldsymbol{\sigma} \bar{\phi} = 0. \end{array} \right. \quad (2b)$$

To make appear the numerical trace  $\hat{u}$ , we need to integrate by parts leading to derivative of  $\mathbf{C}$ .  
 $\Rightarrow$  **when  $\mathbf{C}$  is not constant per cell, one would need to provide its derivative...**



## Variational formulation (2/2): compliance tensor version

$$\text{Using } \mathbf{S} = \mathbf{C}^{-1}, \quad \begin{cases} -\omega^2 \mathbf{u} - \nabla \cdot \boldsymbol{\sigma} = \mathbf{f}, \\ \mathbf{S} : \boldsymbol{\sigma} = \frac{1}{2}(\nabla \mathbf{u} + \nabla^T \mathbf{u}), \end{cases}$$

On each cell  $K_e$  of the mesh,

$$\left\{ \begin{array}{l} \int_{K_e} -\omega^2 \mathbf{u} \bar{\psi} - \int_{K_e} \nabla \cdot \boldsymbol{\sigma} \bar{\psi} = \int_{K_e} \mathbf{f} \bar{\psi}, \end{array} \right. \quad (3a)$$

$$\left\{ \begin{array}{l} \int_{K_e} \frac{1}{2} \nabla \mathbf{u} \bar{\phi} + \int_{K_e} \frac{1}{2} \nabla^T \mathbf{u} \bar{\phi} - \int_{K_e} \mathbf{S} : \boldsymbol{\sigma} \bar{\phi} = 0. \end{array} \right. \quad (3b)$$

⇒ using quadrature formula,  $\mathbf{S}$  can easily vary within cell.

Note that under isotropy, we have an explicit formulation of  $\mathbf{S}$  from Lamé parameters.

## HDG workflow in a nutshell

Unknowns are the discretized variables:  $X^h = (\mathbf{u}^h, \boldsymbol{\sigma}^h)$  and numerical trace  $\hat{\mathbf{u}}^h$ .

$$\left\{ \begin{array}{l} \text{local problem on each cell } K_e : \quad \mathbb{A}_e X_e^h + \mathbb{C}_e \mathcal{R}_e \hat{\mathbf{u}}^h = \mathbb{F}, \\ \text{relation for numerical trace :} \quad \sum_e \mathcal{R}_e^T (\mathbb{B}_e X_e^h + \mathbb{L}_e \mathcal{R}_e \hat{\mathbf{u}}^h) = 0. \end{array} \right.$$

Reorder to write **global problem** in terms of numerical trace only

$$\sum_e \mathcal{R}_e^T (\mathbb{L}_e - \mathbb{B}_e \mathbb{A}_e^{-1} \mathbb{C}_e) \mathcal{R}_e \hat{\mathbf{u}}_h = - \sum_e \mathcal{R}_e^T \mathbb{B}_e \mathbb{A}_e^{-1} \mathbb{F}_e \quad \Leftrightarrow \quad \mathcal{A} \hat{\mathbf{u}}_h = \mathcal{B}.$$

- ① Create local matrices on each cell (embarrassingly parallel) with  $p$ -adaptivity.
- ② Assemble global matrix  $\mathcal{A}$ .
- ③ Solve the large linear system  $\mathcal{A} \hat{\mathbf{u}}^h = \mathcal{B}$  with MUMPS (solve multiple rhs at limited cost).
- ④ Solve the local linear systems to obtain the volume solution  $(\mathbf{u}^h, \boldsymbol{\sigma}^h)$ : (small matrices, embarrassingly parallel,  $< 2\%$  of run time).

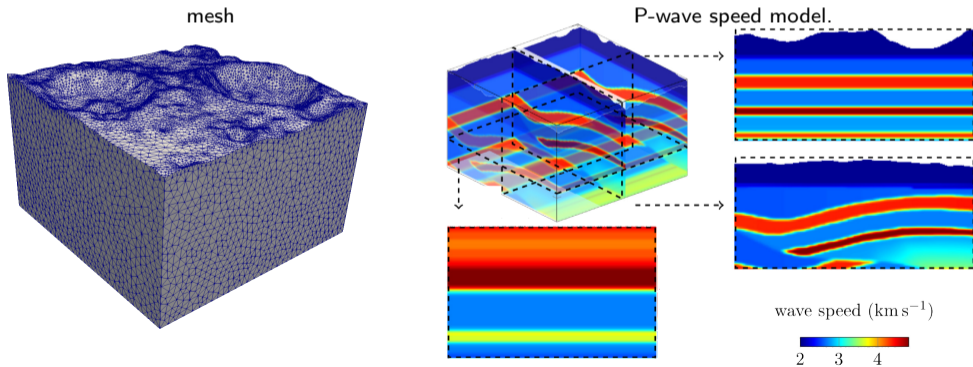
# Plan

- 3 Illustration: Elastic wave propagation with HDG
  - Mathematical formulation and HDG algorithm
  - Illustration of gains

# Elastic-wave propagation with HDG

3D Model with topography, size  $20 \times 20 \times 10 \text{ km}^3$  with topography.

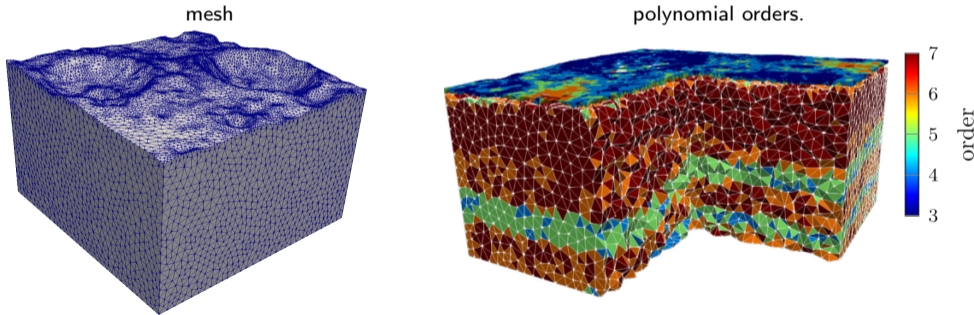
- ▶ Small cells required to accurately describe the topography, *p*-adaptivity
- ▶ Large cells elsewhere to benefit from HDG,
- ▶ models properties vary within the cell, here we use Lagrange basis per cell.



# Elastic-wave propagation with HDG

3D Model with topography, size  $20 \times 20 \times 10$  km<sup>3</sup> with topography.

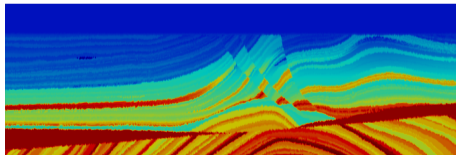
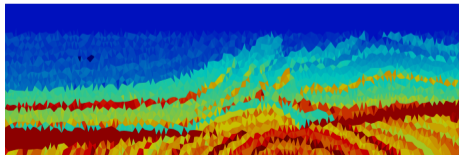
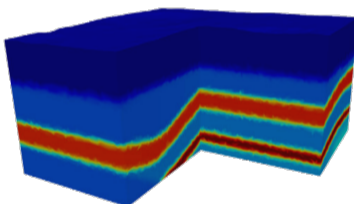
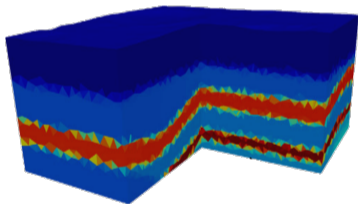
- ▶ Small cells required to accurately describe the topography, *p*-adaptivity
- ▶ Large cells elsewhere to benefit from HDG,
- ▶ models properties vary within the cell, here we use Lagrange basis per cell.



# Elastic-wave propagation with HDG

3D Model with topography, size  $20 \times 20 \times 10$  km<sup>3</sup> with topography.

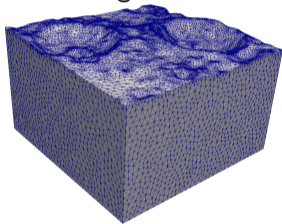
- ▶ Small cells required to accurately describe the topography, *p*-adaptivity
- ▶ Large cells elsewhere to benefit from HDG,
- ▶ models properties vary within the cell, here we use Lagrange basis per cell.



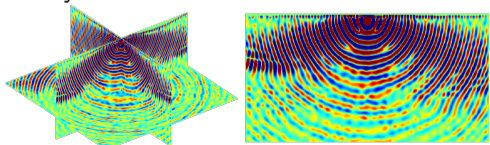
# Matrix size reduction with HDG+MUMPS

3D elastic wave propagation, size  $20 \times 20 \times 10 \text{ km}^3$  with topography.

Mesh using 120 000 cells

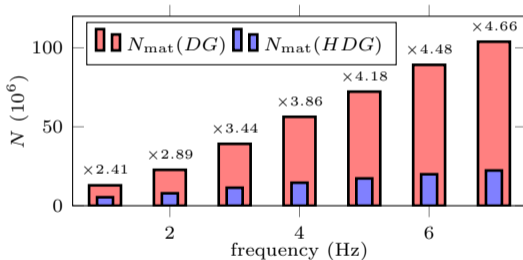


Polynomial order between 2 and 10



displacement field  $u_z$  at 4 Hz

Global matrix size with frequency



elastic simulation 7 Hz with 1600 cores HDG+MUMPS:

- ▶ **matrix size**  $N = 22.3 \times 10^6$ ,
- ▶ **analysis time** 2 min 30 sec,
- ▶ **factorization time** 34 min,
- ▶ **factorization memory** 3589 GiB,
- ▶ **solve time (19 rhs)** 1 min 40 s.

# Plan

## 4 Inverse problem

- Iterative minimization algorithm
- Numerical experiment



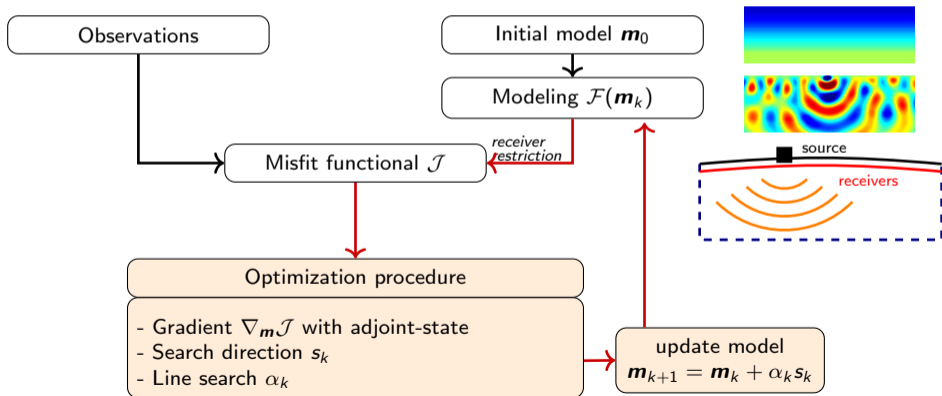
# Plan

- 4 Inverse problem
  - Iterative minimization algorithm
  - Numerical experiment

# Quantitative reconstruction algorithm: FWI

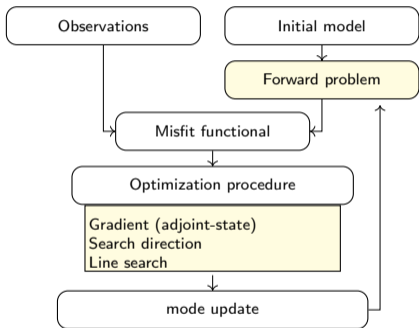
Quantitative reconstruction of properties  $\mathbf{m} = (\lambda, \mu, \rho)$  solving **iterative minimization problem**.

$$\min_{\mathbf{m}} \mathcal{J}(\mathbf{m}) \quad \text{with} \quad \mathcal{J}(\mathbf{m}) = \text{dist}(\mathcal{F}(\mathbf{m}), \mathbf{d}), \quad \mathcal{F}: \text{simulations}, \quad \mathbf{d}: \text{observations}.$$



# Quantitative reconstruction algorithm: FWI

minimize  $\mathcal{J}(\mathbf{m}) = \text{dist}(\mathcal{F}(\mathbf{m}), \mathbf{d})$



- 1 Repeated use of forward wave propagation solver,

$$\begin{cases} \mathbb{A}_e \mathbf{X}_e^h + \mathbb{C}_e \mathcal{R}_e \hat{\mathbf{u}}^h = \mathbb{F}, & (4a) \end{cases}$$

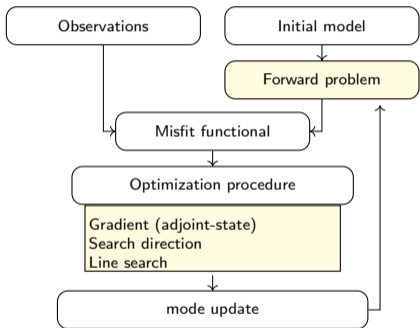
$$\begin{cases} \sum_e \mathcal{R}_e^T (\mathbb{B}_e \mathbf{X}_e^h + \mathbb{L}_e \mathcal{R}_e \hat{\mathbf{u}}^h) = 0. & (4b) \end{cases}$$

- 2 Adjoint-state method for gradient adapted to HDG Lagrangian written from  $\mathcal{J}$  subject to (4a), (4b).

We prove that for HDG, the gradient is still computed from the **adjoint of the direct problem**, fundamental to avoid refactorization of the global matrix.

# Quantitative reconstruction algorithm: FWI

minimize  $\mathcal{J}(\mathbf{m}) = \text{dist}(\mathcal{F}(\mathbf{m}), \mathbf{d})$



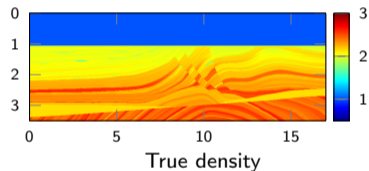
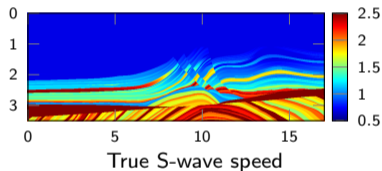
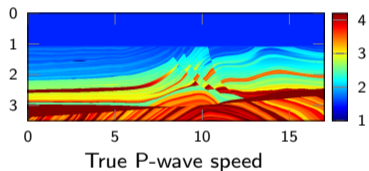
- 1 Repeated use of forward wave propagation solver,
- 2 Adjoint-state method for gradient adapted to HDG,
- 3 To alleviate mesh limitations, the model parameters are represented with Lagrange basis functions.
- 4 Inversion is carried out with respect to the weight of the Lagrange basis functions.

# Plan

- 4 Inverse problem
  - Iterative minimization algorithm
  - Numerical experiment

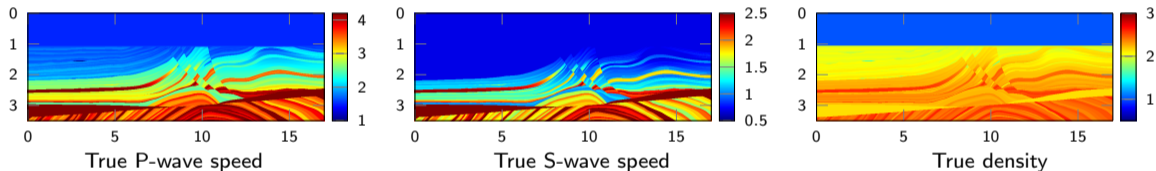
## 2D experiments: Marmousi II setup

We consider the elastic isotropic Marmousi II experiment, of size  $17 \times 3.5 \text{ km}^2$ .  
 Free-surface boundary condition on top and absorbing boundary conditions elsewhere.

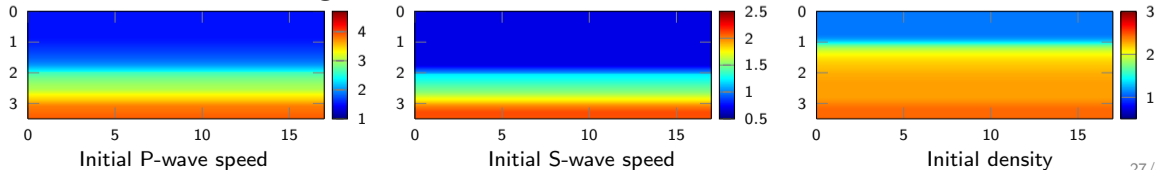


## 2D experiments: Marmousi II setup

We consider the elastic isotropic Marmousi II experiment, of size  $17 \times 3.5 \text{ km}^2$ . Free-surface boundary condition on top and absorbing boundary conditions elsewhere.

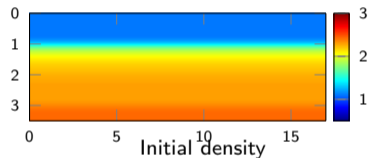
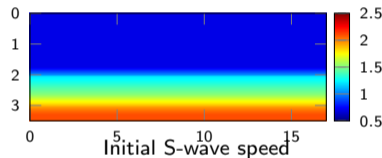
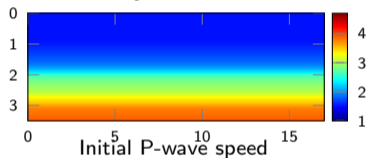


Initial models are 1D-background variation.



## 2D experiments: Marmousi II reconstructions

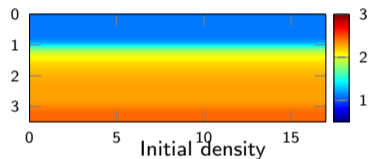
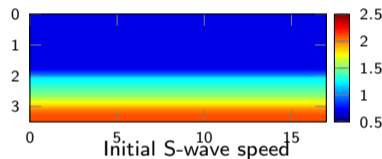
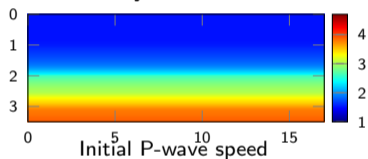
- ▶ Acquisition made up of 169 sources and 849 receivers near surface.
- ▶ Reconstructions using 13 frequencies from 2 to 8 Hz, 25 iterations per frequency.
- ▶ Density is not inverted and remains in its initial value.



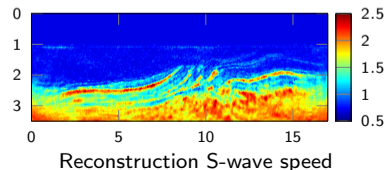
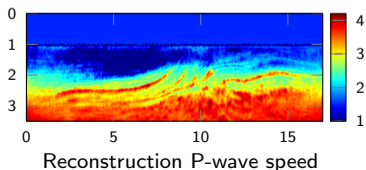


## 2D experiments: Marmousi II reconstructions

- ▶ Acquisition made up of 169 sources and 849 receivers near surface.
- ▶ Reconstructions using 13 frequencies from 2 to 8 Hz, 25 iterations per frequency.
- ▶ Density is not inverted and remains in its initial value.

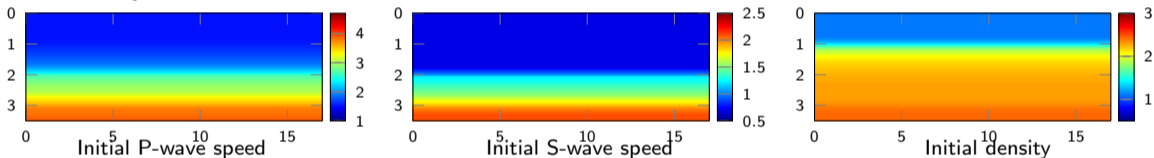


- ▶ Reconstruction using representation in order 1 Lagrange basis per cell ( $\sim 20 \times 10^3$  cells)

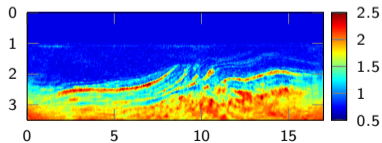


## 2D experiments: Marmousi II reconstructions

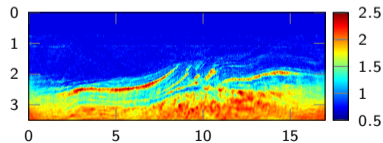
- ▶ Acquisition made up of 169 sources and 849 receivers near surface.
- ▶ Reconstructions using 13 frequencies from 2 to 8 Hz, 25 iterations per frequency.
- ▶ Density is not inverted and remains in its initial value.



- ▶ Computational time ( $18\text{mpi} \times 2\text{omp}$ ):  $2 \cdot 10^4$  cells: 3h;  $5 \cdot 10^4$  cells: 4h15min, i.e. **-30%**.



S-wave speed reconstruction using mesh with 20 000 cells and Lagrange basis representation,



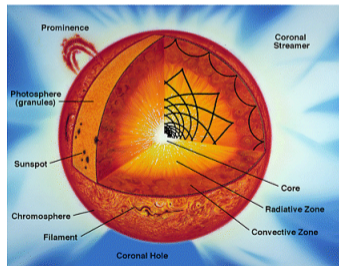
S-wave speed reconstruction using mesh with 50 000 cells piecewise-constant representation.

# Plan

## 5 Helioseismology/asteroseismology

# Helioseismic studies

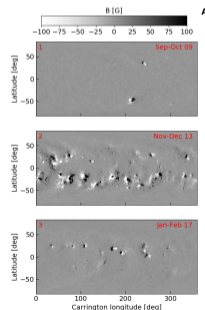
- ▶ Measuring solar/star oscillations,
- ▶ Processing and averaging the observations to extract the seismic data
- ▶ Interpreting the seismic data using forward and inverse methods to estimate solar internal properties.



Solar interior

# Detecting active regions on the far side of the Sun

- ▶ Of great importance for [space-weather forecasts](#)
- ▶ Large active regions that emerge on the Sun's far side will rotate into Earth's view several days later; these may trigger coronal mass ejections, which can [damage satellites and spacecraft and endanger astronauts](#)
- ▶ It is known that far-side imaging can significantly [improve models of the solar wind](#), which plays an important role in space-weather forecasts.



# Numerical simulations of acoustic waves

Acoustic waves propagate horizontally and are trapped in the vertical direction; **they connect the Sun's near and far sides**. As acoustic waves travel faster in magnetized regions, they can inform us about the presence of active regions along their paths of propagation.

Two helioseismic techniques:

- ▶ **Helioseismic holography**: multiply the forward and backward propagated wavefields, and subtract a reference measurement for the quiet Sun.
- ▶ **Time-distance helioseismology**: compute the cross-covariance of the wavefield

**Develop models and computational tools** that are required to recover information about Sun and eventually stellar activity from observations of oscillations.



C. Lindsey and D.C. Braun, Helioseismic holography. [The Astrophysical Journal](#), 1997



L. Gizon, H. Barucq, M. Duruflé, C.S. Hanson, M. Leguèbe, A.C. Birch, J. Chabassier, D. Fournier, T. Hohage and E. Papini, Computational helioseismology in the frequency domain: acoustic waves in axisymmetric solar models with flows. [Astronomy & Astrophysics](#), 2017

# Equations

- **Galbrun's equation** describes adiabatic wave motion subject to source  $F$  with frequency  $\omega$ , on top of a time-invariant fluid background. Ignoring flows and rotation and with Cowling's approximation,

$$-\rho_0(\omega^2 + 2i\omega\Gamma)\xi - \nabla[\gamma p_0 \nabla \cdot \xi] + (\nabla p_0)(\nabla \cdot \xi) - \nabla(\xi \cdot \nabla p_0) + (\xi \cdot \nabla)\nabla p_0 + \rho_0(\xi \cdot \nabla)\nabla \phi_0 = F,$$

with displacement vector  $\xi$  describing the solar oscillation. The density is  $\rho_0$ , pressure  $p_0$ , adiabatic index  $\gamma$ , gravitational potential  $\phi_0$  and attenuation  $\Gamma$ .



H. Barucq, F. Faucher, D. Fournier, L. Gizon and H. Pham, Efficient and accurate algorithm for the full modal Green's kernel of the scalar wave equation in helioseismology. *SIAM J. on Appl. Math.*, 2020.



H. Barucq, F. Faucher, D. Fournier, L. Gizon and H. Pham, Outgoing modal solutions for Galbrun's equation in helioseismology. *J. of Differential Eq.*, 2021, 45

# Equations

- ▶ **Galbrun's equation** describes adiabatic wave motion subject to source  $F$  with frequency  $\omega$ , on top of a time-invariant fluid background. Ignoring flows and rotation and with Cowling's approximation,

$$-\rho_0(\omega^2 + 2i\omega\Gamma)\xi - \nabla[\gamma p_0 \nabla \cdot \xi] + (\nabla p_0)(\nabla \cdot \xi) - \nabla(\xi \cdot \nabla p_0) + (\xi \cdot \nabla)\nabla p_0 + \rho_0(\xi \cdot \nabla)\nabla\phi_0 = F,$$

with displacement vector  $\xi$  describing the solar oscillation. The density is  $\rho_0$ , pressure  $p_0$ , adiabatic index  $\gamma$ , gravitational potential  $\phi_0$  and attenuation  $\Gamma$ .

- ▶ Further approximation ignoring the gravity, we obtain a **scalar-wave equation** for variable  $u := \rho c^2 \nabla \cdot \xi$  such that,

$$-\nabla \cdot \left( \frac{1}{\rho} \nabla u \right) - \frac{\omega^2 + 2i\omega\Gamma}{\rho c^2} u = f, \quad \text{with sound-speed } c.$$



H. Barucq, F. Faucher, D. Fournier, L. Gizon and H. Pham, Efficient and accurate algorithm for the full modal Green's kernel of the scalar wave equation in helioseismology. *SIAM J. on Appl. Math.*, 2020.



H. Barucq, F. Faucher, D. Fournier, L. Gizon and H. Pham, Outgoing modal solutions for Galbrun's equation in helioseismology. *J. of Differential Eq.*, 2021, 45



# Spherical background solar model

## Model S+Atmo: exponentially decreasing density in the solar atmosphere

$$\rho(r) := \begin{cases} \rho_S(r), & r \leq r_a \\ \rho_S(r_a) e^{-\alpha_\infty (r-r_a)}, & r > r_a \end{cases}, \quad c(r) := \begin{cases} c_S(r), & r \leq r_a; \\ c_S(r_a), & r > r_a \end{cases}$$

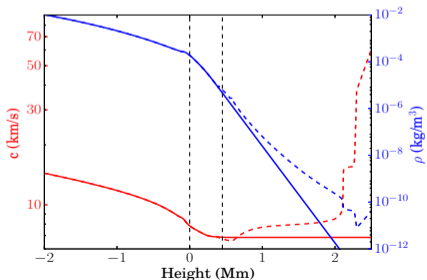
with  $\rho_S > \rho_0 > 0$  ;  $c_S > c_0 > 0$ ,  $R_\odot =$  the solar radius ( $\sim 696 \times 10^3 \text{ km}$ )

# Spherical background solar model

## Model S+Atmo: exponentially decreasing density in the solar atmosphere

$$\rho(r) := \begin{cases} \rho_S(r), & r \leq r_a \\ \rho_S(r_a) e^{-\alpha_\infty (r-r_a)}, & r > r_a \end{cases}, \quad c(r) := \begin{cases} c_S(r), & r \leq r_a \\ c_S(r_a), & r > r_a \end{cases}$$

Comparison of the S+Atmo (solid) and VAL-C (dashed) atmospheric models.



Height above surface (Mm) $R_h$	0.5	0.556	2.543	4
scaled radius = $(R_\odot + R_h)/R_\odot$	1.0007	1.0008	1.0037	1.0058

# Scalar-wave problem formulation, spherical symmetry

$$-\nabla \cdot \left( \frac{1}{\rho} \nabla u \right) - \frac{\omega^2 + 2i\omega\Gamma}{\rho c^2} u = f.$$



H. Barucq, F. Faucher, D. Fournier, L. Gizon and H. Pham, Efficient and accurate algorithm for the full modal Green's kernel of the scalar wave equation in helioseismology. *SIAM J. on Appl. Math.*, 2020.



H. Barucq, F. Faucher, H. Pham, Outgoing solutions and radiation boundary conditions for the ideal atmospheric scalar wave equation in helioseismology. *ESAIM*, 2020.

# Scalar-wave problem formulation, spherical symmetry

$$-\nabla \cdot \left( \frac{1}{\rho} \nabla \mathbf{u} \right) - \frac{\omega^2 + 2i\omega\Gamma}{\rho c^2} \mathbf{u} = \mathbf{f}.$$

① We use the **Liouville transform** to rewrite the problem in Schrödinger form,

With  $u = \rho^{-1/2} \mathbf{u}$  and  $\alpha = -\rho'/\rho$ , we obtain

$$\left( -\Delta - \frac{\omega^2 + 2i\omega\Gamma}{c^2} + \frac{\alpha^2}{4} + \frac{\alpha'}{2} + \frac{\alpha}{r} \right) u = f.$$

In the atmosphere,  $\rho$  is exponentially decreasing  $\Rightarrow \alpha$  is constant.



H. Barucq, F. Faucher, D. Fournier, L. Gizon and H. Pham, Efficient and accurate algorithm for the full modal Green's kernel of the scalar wave equation in helioseismology. *SIAM J. on Appl. Math.*, 2020.



H. Barucq, F. Faucher, H. Pham, Outgoing solutions and radiation boundary conditions for the ideal atmospheric scalar wave equation in helioseismology. *ESAIM*, 2020.

# Scalar-wave problem formulation, spherical symmetry

$$-\nabla \cdot \left( \frac{1}{\rho} \nabla \mathbf{u} \right) - \frac{\omega^2 + 2i\omega \Gamma}{\rho c^2} \mathbf{u} = \mathbf{f}.$$

① We use the **Liouville transform** to rewrite the problem in Schrödinger form,

With  $u = \rho^{-1/2} \mathbf{u}$  and  $\alpha = -\rho'/\rho$ , we obtain

$$\left( -\Delta - \frac{\omega^2 + 2i\omega \Gamma}{c^2} + \frac{\alpha^2}{4} + \frac{\alpha'}{2} + \frac{\alpha}{r} \right) u = f,$$

In the atmosphere,  $\rho$  is exponentially decreasing  $\Rightarrow \alpha$  is constant.

② Allows us to build the exact Dirichlet-to-Neumann map and new classes of Radiation Boundary conditions for outgoing solutions.



H. Barucq, F. Faucher, D. Fournier, L. Gizon and H. Pham, Efficient and accurate algorithm for the full modal Green's kernel of the scalar wave equation in helioseismology. *SIAM J. on Appl. Math.*, 2020.



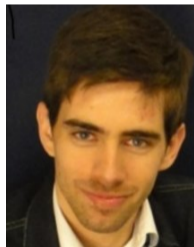
H. Barucq, F. Faucher, H. Pham, Outgoing solutions and radiation boundary conditions for the ideal atmospheric scalar wave equation in helioseismology. *ESAIM*, 2020.

# Plan

- 6 Illustration: Green's function computations for time-distance helioseismology
  - Modal Green's kernel
  - Numerical experiments
  - Power spectrum, comparison with measured data
  - The vector wave problem

# Numerical method for computing Green's functions

In collaboration with Florian Faucher, Ha Pham, and Damien Fournier, Laurent Gizon from Max Planck Institute for Sun (MPS, Göttingen, Germany)



## Cross-covariance in terms of Green's function

At frequency  $\omega$ , consider the cross-covariance in Fourier space as the product of the wave field at two locations of measurement,

$$C(r_1, r_2, \omega) = \Psi^*(r_1, \omega)\Psi(r_2, \omega)$$

Here,  $\Psi = c\nabla \cdot \xi$ . In terms of the Green's function, we have

$$\Psi(r_j, \omega) = \int_V G(r_j, r, \omega)s(r, \omega)\rho dr$$

where the source  $s(r, \omega)$  is a realization of a random process.



# Plan

## 6 Illustration: Green's function computations for time-distance helioseismology

- Modal Green's kernel
- Numerical experiments
- Power spectrum, comparison with measured data
- The vector wave problem

## Modal Green's kernel

Decomposition on harmonic mode  $\ell$ , the modal Green's kernel  $G_\ell$  solves,

$$\mathcal{L} G_\ell(r, s) = \delta(r - s), \quad \text{with} \quad \mathcal{L} := \left( -\partial_r^2 - \frac{\omega^2 + 2i\omega\Gamma}{c^2} + \frac{\alpha^2}{4} + \frac{\alpha'}{2} + \frac{\alpha}{r} + \frac{\ell(\ell+1)}{r^2} \right).$$

with Neumann boundary condition at origin:

$$\partial_n G_\ell(r=0) = 0,$$

and radiation condition at  $r = r_{\max}$ :

$$(\partial_n G_\ell - \mathcal{Z} G_\ell)_{r=r_{\max}} = 0.$$



H. Barucq, F. Faucher, H. Pham, *Outgoing solutions and radiation boundary conditions for the ideal atmospheric scalar wave equation in helioseismology.* ESAIM, 2020.

# Modal Green's kernel

Decomposition on harmonic mode  $\ell$ , the modal Green's kernel  $G_\ell$  solves,

$$\mathcal{L} G_\ell(r, s) = \delta(r - s), \quad \text{with } \mathcal{L} := \left( -\partial_r^2 - \frac{\omega^2 + 2i\omega\Gamma}{c^2} + \frac{\alpha^2}{4} + \frac{\alpha'}{2} + \frac{\alpha}{r} + \frac{\ell(\ell + 1)}{r^2} \right).$$

with Neumann boundary condition at origin:

$$\partial_n G_\ell(r = 0) = 0,$$

and radiation condition at  $r = r_{\max}$ :

$$(\partial_n G_\ell - \mathcal{Z} G_\ell)_{r=r_{\max}} = 0.$$

## Computation of the modal Green's kernel:

- ▶ **Approach 1 (naive):** for each source position  $s$ , solving equation  $\mathcal{L} G_\ell(r, s) = \delta(r - s)$  gives  $G_\ell(\cdot, s)$ .
- ▶ **Approach 2:** Use an assembling formula, the entire kernel is obtained from the solutions of only two boundary-value problems.



## Computation of the Green's kernel: Approach 2

- ▶ **Approach 1 (naive):** for each source position  $s$ , solve equation  $\mathcal{L} G_\ell(r, s) = \delta(r - s)$ .
- ▶ **Approach 2:** Use an assembling formula, the entire kernel is obtained from the solutions of only two boundary-value problems.

- ① Find  $\psi_1$  that solves
 
$$\begin{cases} \mathcal{L} \psi_1 = 0, & \text{on } (0, r_{\max}), \\ (\partial_n \psi_1)_{r=0} = 0, & (\psi_1)_{r=r_b} = 1. \end{cases}$$
- ② Find  $\psi_2$  that solves
 
$$\begin{cases} \mathcal{L} \psi_2 = 0, & \text{on } (r_a, r_{\max}), \\ (\psi_2)_{r=r_a} = 1, & (\partial_n \psi_2 - \mathcal{Z} \psi_2)_{r=r_{\max}} = 0. \end{cases}$$



H. Barucq, F. Faucher, D. Fournier, L. Gizon and H. Pham, Efficient and accurate algorithm for the full modal Green's kernel of the scalar wave equation in helioseismology. *SIAM J. on Appl. Math.*, 2020.

## Computation of the Green's kernel: Approach 2

- ▶ **Approach 1 (naive):** for each source position  $s$ , solve equation  $\mathcal{L} G_\ell(r, s) = \delta(r - s)$ .
- ▶ **Approach 2:** Use an assembling formula, the entire kernel is obtained from the solutions of only two boundary-value problems.

- 1 Find  $\psi_1$  that solves
 
$$\begin{cases} \mathcal{L} \psi_1 = 0, & \text{on } (0, r_{\max}), \\ (\partial_n \psi_1)_{r=0} = 0, & (\psi_1)_{r=r_b} = 1. \end{cases}$$
- 2 Find  $\psi_2$  that solves
 
$$\begin{cases} \mathcal{L} \psi_2 = 0, & \text{on } (r_a, r_{\max}), \\ (\psi_2)_{r=r_a} = 1, & (\partial_n \psi_2 - \mathcal{Z} \psi_2)_{r=r_{\max}} = 0. \end{cases}$$

- 3 Assemble the Green's kernel, with  $H$  the Heaviside and  $\mathcal{W}$  the Wronskian
 
$$\mathcal{W}(s) := \mathcal{W}\{\psi_1(s), \psi_2(s)\},$$

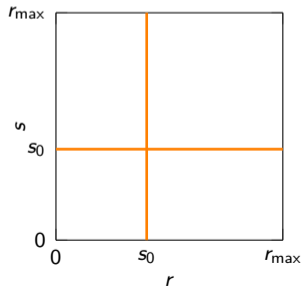
$$G_\ell(r, s) = \frac{-H(s - r) \psi_1(r) \psi_2(s) - H(r - s) \psi_1(s) \psi_2(r)}{\mathcal{W}(s)}, \quad \forall (r, s) \in (r_a, r_{\max}),$$



# Computation of the Green's kernel: Approach 2

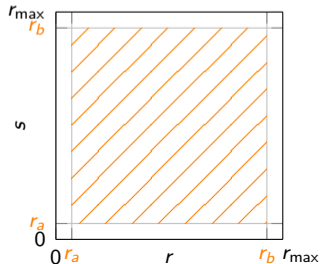
- ▶ **Approach 1 (naive):** for each source position  $s$ , solve equation  $\mathcal{L} G_\ell(r, s) = \delta(r - s)$ .
- ▶ **Approach 2:** Use an assembling formula, the entire kernel is obtained from the solutions of only two boundary-value problems.

**Approach 1:** the solution of one problem for a Dirac in  $s_0$  only gives  $G_\ell(r, s = s_0)$  and  $G_\ell(r = s_0, s)$ .



**Approach 2:** from the solutions of two boundary value problems,  $G_\ell(r, s)$  is obtained for any position between  $r_a$  and  $r_b$ .

It also avoids the singularity of the Dirac source.

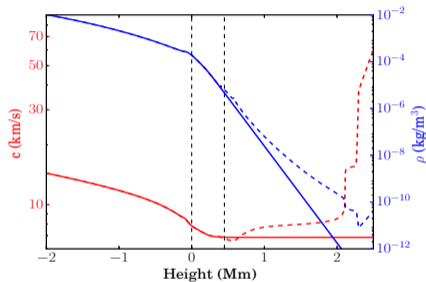


# Plan

- 6 Illustration: Green's function computations for time-distance helioseismology
  - Modal Green's kernel
  - Numerical experiments
  - Power spectrum, comparison with measured data
  - The vector wave problem

# Solar Green's kernels

- ▶ The background sound-speed and density are given by model S+Atmo or model Val-C.

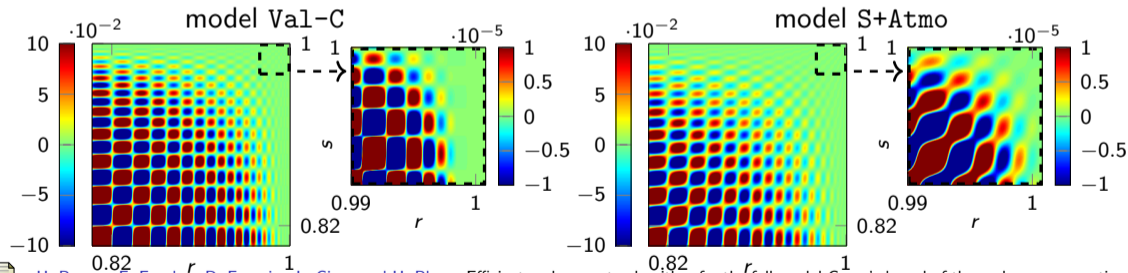




# Solar Green's kernels

- ▶ The background sound-speed and density are given by model S+Atmo or model Val-C.
- ▶ The Green's kernel is computed with Approach 2 which only need the solutions of two problems.

Imaginary part of the Solar modal Green's functions at 7 mHz for mode  $\ell = 100$  using different background.



H. Barucq, F. Faucher, D. Fournier, L. Gizon and H. Pham, Efficient and accurate algorithm for the full modal Green's kernel of the scalar wave equation in helioseismology. *SIAM J. on Appl. Math.*, 2020



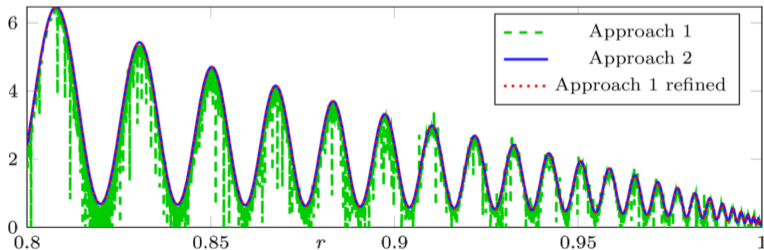
F. Faucher  
hawen: time-harmonic wave modeling and inversion using hybridizable discontinuous Galerkin discretization  
*Journal of Open Source Software*, 6 (57), 2021

# Solar Green's kernels

- ▶ The background sound-speed and density are given by model S+Atmo or model Val-C.
- ▶ The Green's kernel is computed with Approach 2 which only needs the solutions of two problems.

Approach 2 is more **efficient** as it only needs two boundary value problems to assemble the entire kernel, and more **accurate** as it avoids the Dirac singularity.

- 1 To obtain  $G_\ell(s, s)$  with Approach 1, we need 4000 simulations,
- 2 Approach 1 needs a refined discretization mesh to capture correctly the singularity.



# Plan

- 6 Illustration: Green's function computations for time-distance helioseismology
  - Modal Green's kernel
  - Numerical experiments
  - Power spectrum, comparison with measured data
  - The vector wave problem

# Power spectrum

Observables are an average over height of  $G_\ell$ , in first approximation (depending on the assumption on the source), one can consider the Power Spectrum to be directly related to the Imaginary part of  $G_\ell$ ,

$$\mathcal{P}_\ell(\omega) \propto \left| \text{Im}(G_\ell(\omega)(r_0, s_0)) \right|^2. \tag{9}$$

We can compare the numerical power spectrum, i.e., using Green's function computed for harmonic degrees (modes)  $\ell$  and frequencies  $\omega/(2\pi)$ , with observations.

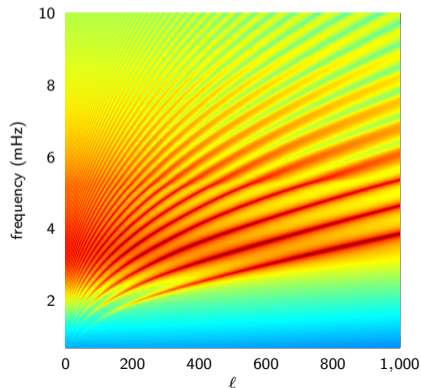


H. Barucq, F. Faucher, D. Fournier, L. Gizon and H. Pham, Efficient and accurate algorithm for the full modal Green's kernel of the scalar wave equation in helioseismology. *SIAM J. on Appl. Math.*, 2020.

# Power spectrum

We evaluate the imaginary part of the Green's function  $G_\ell(r = 1, s = 1)$  with frequencies and modes, using model S+Atmo.

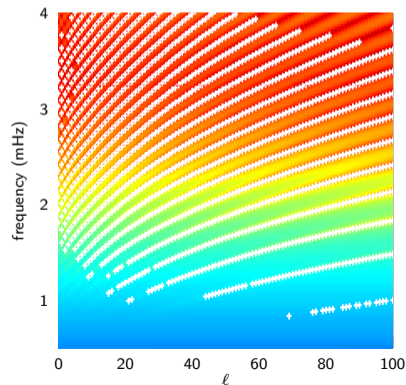
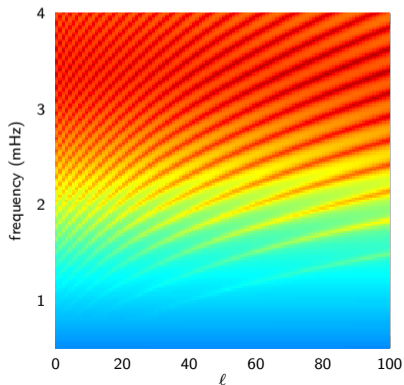
$$\ell \in (0, 1000), \quad \omega/(2\pi) \in (0, 10)\text{mHz}.$$



# Power spectrum

We evaluate the imaginary part of the Green's function  $G_\ell(r = 1, s = 1)$  with frequencies and modes, using model S+Atmo.

Comparison with HMI data (white crosses), for  $\ell \in (0, 100)$ ,  $\omega/(2\pi) \in (0.5, 4)\text{mHz}$ .



# Plan

- 6 Illustration: Green's function computations for time-distance helioseismology
  - Modal Green's kernel
  - Numerical experiments
  - Power spectrum, comparison with measured data
  - The vector wave problem

## Vector-wave equation with gravity

The same method can be applied to the vector-wave problem (Vector Spherical Harmonics),

$$-\rho_0(\omega^2 + 2i\omega\Gamma)\xi - \nabla[\gamma p_0 \nabla \cdot \xi] + (\nabla p_0)(\nabla \cdot \xi) - \nabla(\xi \cdot \nabla p_0) + (\xi \cdot \nabla)\nabla p_0 + \rho_0(\xi \cdot \nabla)\nabla \phi_0 = F,$$

That is, the vector Green's kernels (depending on the direction) can be obtained from the computation of only two boundary-value problems.



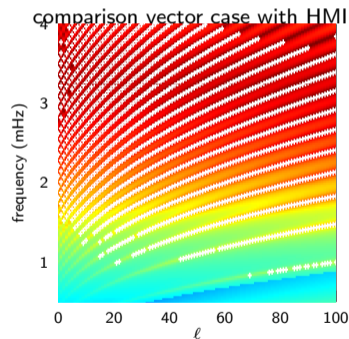
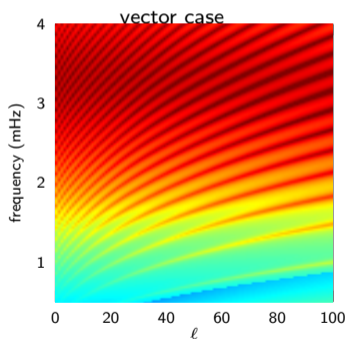
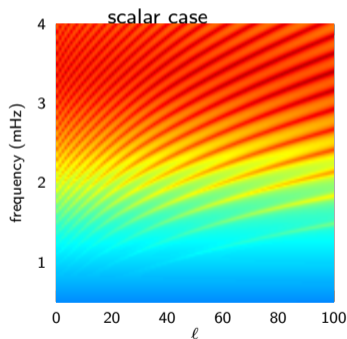
H. Barucq, F. Faucher, D. Fournier, L. Gizon and H. Pham, Efficient computation of modal Green's kernels for vectorial equations in helioseismology under spherical symmetry. [Research Report, 2021.](#)



# Vector-wave equation with gravity

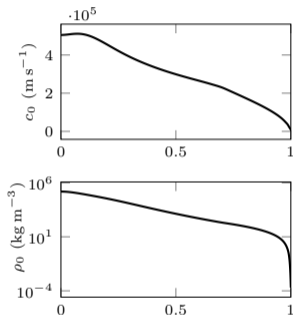
Comparison with HMI data (white crosses), for  $\ell \in (0, 100)$ ,  $\omega/(2\pi) \in (0.5, 4)\text{mHz}$ .

**Including the gravity effect, f and g-modes now appear.**

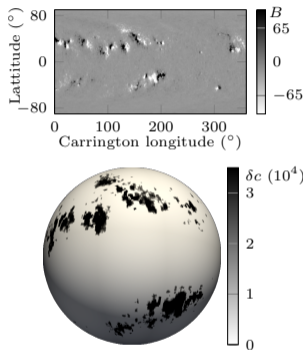


H. Barucq, F. Faucher, D. Fournier, L. Gizon and H. Pham, Efficient computation of modal Green's kernels for vectorial equations in helioseismology under spherical symmetry. [Research Report, 2021](#).

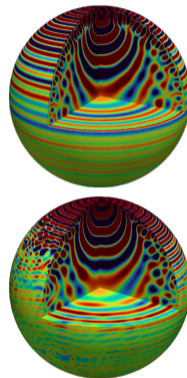
# Towards 3D simulations



(a) spherical solar background models



(b) Active region as velocity perturbation



(c) Simulations with spherical background (top) and perturbations (bottom).

Scalar-wave propagation in global 3D Sun with in-house code hawen. The memory cost for its factorization is of 3 TiB.

# Plan

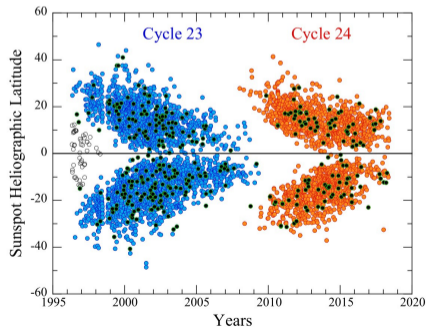
## 7 Conclusion

# Recap

- ▶ Simulation of wave propagation provides a non invasive tool for probing the invisible
- ▶ Advanced numerical methods and HPC are mandatory
- ▶ Inversion remains very sensitive
- ▶ Recovering real data is also very sensitive and mathematical modeling has its part to play

# Ongoing works

- ▶ Coupling SEM and DG for time-dependent problems in geophysics
- ▶ Conducting porous media
- ▶ Imaging 3D anisotropic elastic media with new acquisition methods (DAS)
- ▶ Solve the 3D Galbrun's equation with and without Cowling's approximation
- ▶ Construction of Butterfly diagrams for stars
- ▶ and so many very exciting problems



# Makutu, September 2022



THANK YOU